In Situ Printing-then-Mixing for Biological Structure Fabrication using Intersecting Jets

Kyle Christensen[1], Ashley Compaan[2], Wenxuan Chai[1], Guangbin Xia[3], Yong Huang[1,2,4,*]

[1] Department of Mechanical and Aerospace Engineering, University of Florida, Gainesville, FL 32611, USA

[2] Department of Materials Science and Engineering, University of Florida, Gainesville, FL 32611, USA

[3] Department of Neurology, University of Florida, Gainesville, FL 32611, USA

[4] Department of Biomedical Engineering, University of Florida, Gainesville, FL 32611, USA

* Corresponding author, P.O. Box 116250, University of Florida, Gainesville, FL 32611, USA, Phone: 001-352-392-5520, Fax: 001- 352-392-7303, Email: yongh@ufl.edu

Abstract

While traditional three-dimensional bioprinting technology is suitable for many tissue engineering applications, various biomaterials and constructs call for bioprinting innovations. There is a need for the fabrication of complex structures from reactive biomaterials as well as heterogeneous structures with controlled material compositions. In particular, during reactive material printing, reactive solutions/suspensions which undergo changes in rheological properties or cytocompatibility are not printable using traditional bioprinting approaches which require all components of bioinks to be mixed before deposition. The objective of this study is to develop and implement an intersecting jets-based inkjet bioprinting approach, which enables voxel-

resolution printing-then-mixing for the fabrication of biological structures using reactive materials as well as structures having a compositional gradient. Inkjetting is implemented herein as a versatile technique to simultaneously deposit droplets of disparate materials at controlled locations where active collision, mixing, and coalescence occur. For reactive material printing, neural stem cell (NSC) spheres are fabricated from reactive PuraMatrix hydrogel solution and physiological cell suspension, and cell-laden alginate structures are also printed in air directly from reactive sodium alginate and calcium chloride solutions. For heterogeneous structure printing, collagen sheets with a hydroxyapatite (HAP) content gradient are fabricated to demonstrate the unique online control of material composition throughout a structure. It is demonstrated that the proposed bioprinting approach is feasible for applications which utilize reactive materials or require heterogeneous compositions.

Keywords: inkjet bioprinting; intersecting jets; reactive materials; neural stem cell; alginate; hydroxyapatite

1. Introduction

The fabrication of human tissue constructs has been a technical challenge requiring advanced manufacturing techniques. Additive manufacturing for healthcare applications, or three-dimensional (3D) bioprinting, has made great developmental strides in recent decades and aims to fabricate bioactive or living cellular structures[1]. With user-defined geometry, materials, and cellular composition, printed biological structures offer great promise as regenerative medicine and tissue engineering platforms for the study of disease progression and drug efficacy, to name a few[2]. Furthermore, the on-demand fabrication of implantable tissues for the repair or

replacement of organs offers a viable solution to address the growing shortage of organ donors and transplantable human organs[1,3].

While various materials have been utilized with bioprinting approaches, some biomaterials ideal for tissue engineering applications are not printable using the traditional mixing-then-printing approach, which requires all components of bioinks, including soluble components such as matrix precursors and suspended materials such as living cells, to be mixed before deposition. For these materials, the matrix precursor rapidly becomes unprintable due to significant rheological changes resulting from the physiological conditions (temperature, ionic strength, pH) required to maintain cell viability during the printing process. While the material may be printable using cytotoxic ink formulations, the fabrication of cell laden structures utilizing such materials is not feasible.

Generally, bioprinting approaches can be classified as droplet-based, including inkjet[4-9] and laser-induced forward transfer[10,11] printing, or filament-based, including microextrusion[12,13] and filament assembly[14,15]. For voxel-resolution bioprinting, droplet-based printing techniques are often favored[4-9,16-18] for their low cost, scalability, and high resolution[2], and reactive solutions/suspensions may be utilized for printing-then-mixing fabrication approaches in which droplets interact in air or on a substrate. Among various droplet-based printing techniques, inkjetting-based mixing has been achieved by alternating printing, in which droplets are deposited at the same location/layer sequentially with a substantial time interval between impacts[16-19], and simultaneous printing, in which droplets collide at the same location at the same time[20-24]. Alternating printing of reactive materials has been implemented for the fabrication of droplet arrays with gradients in cell concentrations[16], 3D cellular hydrogel structures[17,18], and droplets of synthesized nylon 6[19]. However, alternating printing requires that deposition

locations are precisely known and controlled, such that droplets impact onto one another after a controlled movement between printheads. This alignment may be difficult and is subject to error and fluctuations in jet trajectory[19]. While the approach is scalable, the frequent need to move printheads between deposition locations for each deposited droplet increases the time required to fabricate structures and may be incompatible with typically used deposition frequencies ranging from tens to hundreds of hertz[5,6,8]. Sequential deposition may also not be suitable for printing approaches which utilize a solution bath to crosslink and support structures during printing[4-6]. Due to the time between alternating ink depositions, one initially printed ink may be diluted by, react with, or diffuse into the surrounding bath before its reactive counterpart is printed, preventing mixing or interaction with subsequently printed material.

Simultaneous printing of reactive materials may overcome these limitations, and droplet-based approaches have utilized the collision of reactive droplets in air to fabricate microcapsules using inclined microdispensers[20], an ultrasonic atomizer[21,22], a twin-head electrospraying system with opposite charges[23], or spray dried coaxial fluid flows[24]. However, the deposition location of droplets after impact in air was not controllable, especially for spray-based techniques, such that these approaches may not be applicable for 3D structure fabrication.

Beyond the printing of reactive materials, inkjet printing-based printing-then-mixing also offers potential for the fabrication of structures with gradients of cells, different materials, or growth factors throughout[2]. However, cellular and material spatial heterogeneity as occurs in native tissues is yet to be achieved, as structures are typically fabricated by printing a single bioink[4-6,8]. Cellular heterogeneity within a structure has been demonstrated by depositing different cell-laden solutions in discrete regions[7], but this approach is limited by the drawbacks of alternating deposition. Similarly, gradients in cell types and density have been achieved by

patterning cells[25] and growth factors[26,27] in two-dimensional arrays, but approaches are again based on alternating deposition and may fall short of complete mixing of deposited materials. Conversely, the ability to simultaneously deposit materials at varying ratios would enable online control of material composition and facilitate the fabrication of structures with numerous applications including flexible electronics, sensors, soft robots, and structural composites in addition to tissue engineering[28].

The objective of this study is to develop and implement an intersecting jets-based inkjet bioprinting approach, which enables voxel-resolution printing-then-mixing for the fabrication of biological structures using reactive materials as well as structures having a compositional gradient. Utilizing the proposed system, structures can be fabricated utilizing reactive biomaterials which are not compatible with traditional bioprinting approaches. That is, materials which undergo a loss of printability or cytocompatibility when mixed prior to deposition, as is required by traditional printing approaches, are compatible with the proposed printing-then-mixing approach. Additionally, the intersecting jets approach offers online voxel-level control of the local composition of printed structures. That is, structures with compositional gradients or arbitrarily varying material composition may be fabricated by controlling the ratio of deposited materials at any point within a structure. It is noted that filament-based printing has been used to fabricate 3D structures from reactive materials and with compositional gradients using active mixing immediately prior to deposition such that the timescale of mixing is shorter than the reaction timescale[28]. However, voxel-level control of composition is not achievable and materials which rapidly undergo changes in rheological properties or cytocompatibility may be incompatible with the extrusion approach. The feasibility of the intersecting jets approach proposed herein is demonstrated by printing the following structures: 1) neural stem cell (NSC)

spheres from a reactive PuraMatrix hydrogel solution and a physiological cell suspension which are incompatible with traditional printing approaches; 2) cell-laden alginate structures from reactive sodium alginate and calcium chloride solutions without the use of a traditional crosslinking bath; and 3) collagen structures with a hydroxyapatite (HAP) content gradient not readily achievable by traditional printing approaches. Since the primary goal of their fabrication herein is to illustrate the unique biofabrication capabilities of the intersecting jets-based printing approach, intensive biological investigation of these printed structures is not conducted in this study.

2. Materials and Methods

2.1. Intersecting jets printing platform

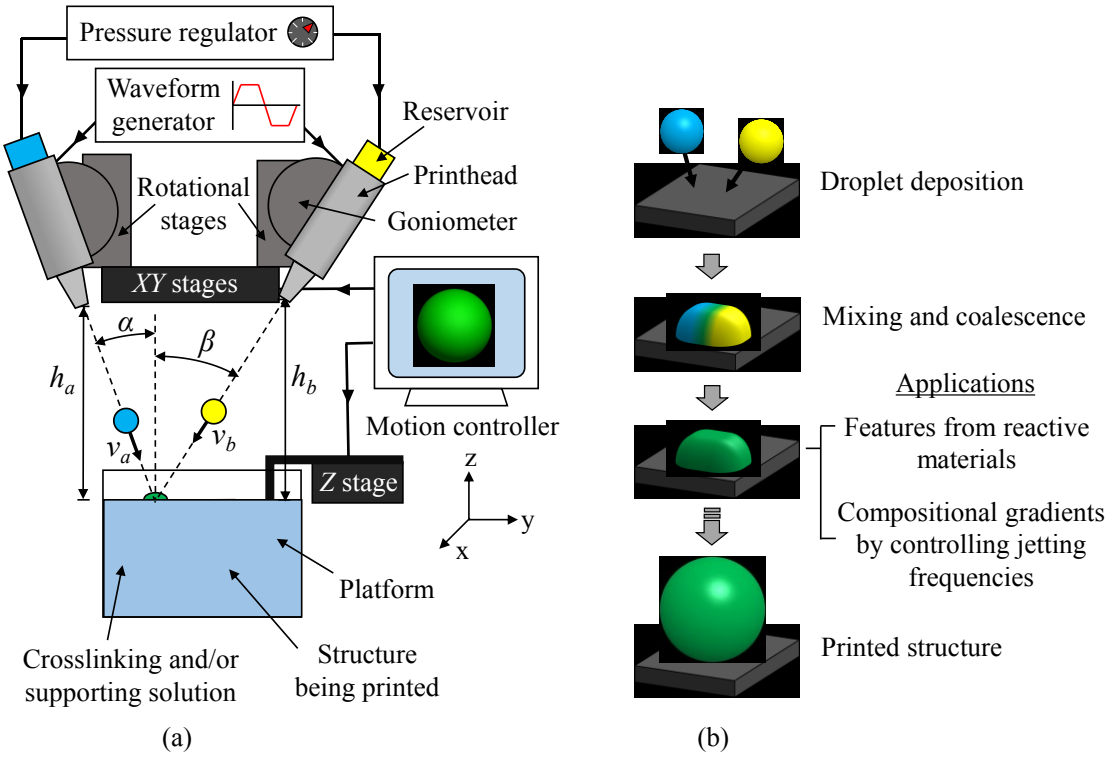

Fig. 1. (a) Printing schematic and (b) printing sequence illustrating the intersecting jets approach. Key components are shown and process variables are identified.

The proposed intersecting jets approach was developed and implemented based on a platform-assisted 3D inkjet printing setup[6]. As illustrated in Fig. 1, the intersecting jets printing system had three key modules: the droplet generation module, the motion control module, and the jet alignment module. The droplet generation module was responsible for the formation of droplets of reactive material fluids. Herein droplets were ejected in a drop-on-demand mode[29] using 120 μm diameter MJ-ABL piezoelectric printheads (MicroFab, Plano, TX), with driving voltages between ± 60 and ± 120 V, rise and fall times of 6 μs, dwell/echo times of 20-45 μs, and frequencies of 30-120 Hz. Fluid back pressures were maintained using a multichannel pneumatics controller (MicroFab, Plano, TX) to ensure proper menisci within the nozzles for droplet formation. The motion control module coordinated the motion of the printheads and receiving platform. During printing, the printheads were fixed relative to one another and moved in the *xy* plane relative to the platform; the platform, where the printed structure was built, provided the *z*-direction motion to match the layer thickness. The deposition location of droplets was controlled by computerized movement of the printheads such that adjacent droplets formed layers of designed shapes. For typical support bath-enabled printing[8], layers were solidified as the structure was submerged into a crosslinking and supporting solution. For printing in air, structures were printed directly onto a receiving glass slide. Based on a computer aided design (CAD), layers were printed on top of one another consecutively to form a 3D structure. In particular, the printhead motion was controlled by motorized *xy* stages (Aerotech, Pittsburgh, PA) and the receiving platform was lowered by a *z* stage (Aerotech, Pittsburgh, PA). The motion of the *xyz* stages was controlled using AeroBasic and G code commands based on the designed geometry. Printhead travel speeds ranged from 1 to 8 mm/s, and layer thickness was controlled at 25 or 50 μm.

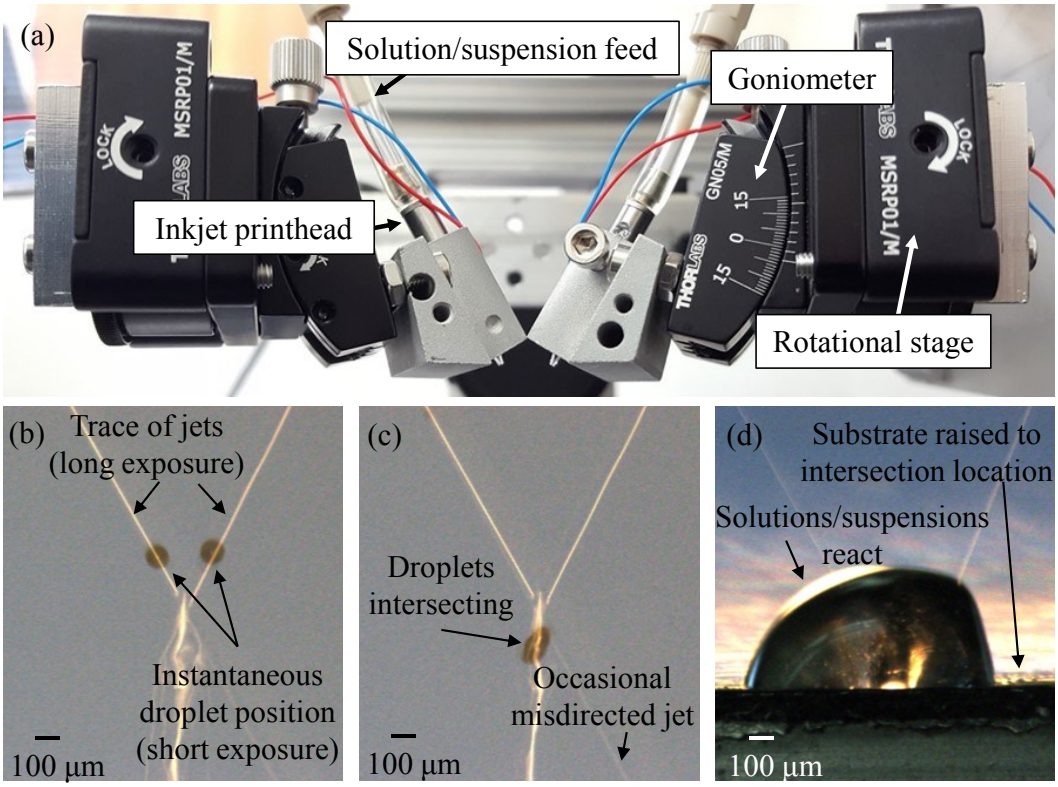

Fig. 2. (a) Components of the intersecting jets alignment module and time-resolved imaging of jet intersection in air showing two droplets (b) before and (c) after collision as well as traces of their respective paths, and (d) the deposition of intersected droplets.

The jet alignment module was designed to control the alignment and collision of generated droplets. As shown in Fig. 1, jets from two inclined printheads, which may have different standoff distances (h_a and h_b) but were fixed at 5.0 mm for both printheads in this study, and different inclination angles (α and β) but were fixed at 30 degrees for both printheads in this study, were aligned such that droplets intersected at a deposition location at speeds of v_a and v_b. For the alignment of multiple inkjet printheads, a customized goniometer-based apparatus was

designed and fabricated. As shown in Fig. 2(a), the apparatus had a frame with linear slots for adjustment of the distances between the printheads. The printheads were mounted to goniometers (Thorlabs, Newton, NJ), which were further mounted to rotational stages (Thorlabs, Newton, NJ), respectively. The rotational stages controlled the rotation angle of each printhead while the goniometers controlled the inclination angle of each printhead. The final deposition location of each jet was determined by the combined effects of the slot, goniometer, and rotational stage orientations. During printing, the linear slots were adjusted once to achieve the desired proximity between printheads. The goniometers and rotational stages were then adjusted in conjunction to align each jet as desired. A time-resolved imaging system (MicroFab, Plano, TX) was used to observe jet orientations and ensure the collision of printed droplets. By controlling the delay between the activation of a strobe and the generation of droplets, droplet positions were observed during flight as illustrated in Fig. 2. Strobe delay and activation was controlled by the multichannel waveform generator, and droplets were observed using a color camera (Sentech, Carrollton, TX).

Typical printing operation was commenced by achieving consistent jet intersection as observed by the time-resolved imaging system by adjusting the goniometer and rotational stage of each printhead. With stroboscopic alignment and feedback to control jet intersection, inconsistencies in jet trajectory are less problematic compared to sequential deposition techniques. Figure 2(b) and (c) shows time-resolved imaging of the alignment of two intersecting jets and the impact of droplets in air. Illuminated intersecting lines illustrate the trace of jets using long exposure time. When consistent jet intersection was achieved, the printing substrate was raised to the intersection height as shown in Fig. 2(d) for printing.

2.2. Printing protocol

A typical printing process involves two key phases: jet alignment and 3D printing. During the jet alignment phase, the droplet formation conditions[29] for each printhead are first tuned for the best jetting and droplet formation performance based on the rheological properties of each reactive material fluid. Then consistent jet intersection is achieved by adjusting the goniometer and rotational stage of each printhead. During the 3D printing phase, the deposition location of the intersecting jets is controlled along designed paths to form a layer. As each layer is deposited, the substrate is lowered by the vertical thickness of the printed layer. For typical support bath-enabled inkjet bioprinting[8], each printed layer on the platform is submerged into a solution, which both crosslinks and mechanically supports the structure being printed. Subsequent layers of the structure are then printed on top of the previous layers and again submerged after deposition. For printing in air, printing and crosslinking occur directly on a receiving substrate.

2.3. 3D printing applications and materials

To illustrate the feasibility of the proposed intersecting jets-based printing approach, it was applied to the printing of reactive materials as well as the fabrication of heterogeneous structures. For reactive material printing, neural stem cell (NSC) spheres were fabricated from a reactive PuraMatrix hydrogel solution and a physiological cell suspension, and cell-laden alginate structures were also printed in air directly from reactive sodium alginate and calcium chloride solutions. For heterogeneous structure printing, collagen sheets with a hydroxyapatite (HAP) content gradient were fabricated to demonstrate the unique online control of material composition throughout a structure.

2.3.1 NSC sphere printing and materials

The ability to fabricate structures from reactive materials using intersecting jets was demonstrated by printing PuraMatrix spheres encapsulating neural stem cells (NSC). PuraMatrix is a self-assembling peptide polymer and forms a hydrogel desirable for encapsulating NSC and other cell lines[30-32] at physiological pH. In this study, PuraMatrix was utilized to encapsulate NSCs within spheres. PuraMatrix is not compatible with traditional single-printhead inkjet bioprinting as it is only printable as a low viscosity acidic solution, precluding the suspension of cells and limiting its applications for bioprinting. As such, there is a need to print NSC spheres using the proposed intersecting jets printing approach.

DM03-NSCs derived from human myotonic dystrophy type 1 induced pluripotent stem (iPS) cells (Guangbin Xia's lab, Department of Neurology, University of Florida, Gainesville, FL) were cultured as described elsewhere.[33,34] Briefly, NSCs were maintained in Dulbecco's Modified Eagles Medium (DMEM) (Corning Cellgro, Manassas, VA) supplemented with 20% Fetal Bovine Serum (FBS) (HyClone, Logan, UT) in a humidified 5% CO_2 incubator at 37°C, and the culture medium was replaced every 3 days as required. To prepare NSC bioink for printing, freshly 90% confluent flasks were washed twice with phosphate-buffered saline (PBS) without calcium and magnesium (Corning Cellgro, Manassas, VA), and incubated with 0.25% trypsin/EDTA (Gibco, Grand Island, NY) for 5 min at 37°C to detach the cells from the culture flasks. 10 mL of complete cell medium was added to the cell suspension which was centrifuged at 1,000 rpm for 5 minutes at room temperature, and the resulting pellet was resuspended in PBS to a final concentration of 5×10^6 cells/mL. PBS without calcium was used as the presence of calcium facilitates rapid formation of NSC aggregates which may clog the nozzle during printing. PuraMatrix (Discovery Labware Inc., Bedford, MA) was diluted to a concentration of

0.4% (w/v) using deionized (DI) water. Finally, the 5×10^6 cell/mL NSC suspension was prepared as one ink, and the 0.4% PuraMatrix solution was the other ink for fabrication. Two types of NSC spheres (2 and 3 mm in diameter) were printed using deposition frequencies of 30 Hz for both inks, a constant printhead travel speed of 7.2 mm/s, and a layer thickness of 25 μm.

2.3.2 Alginate structure printing in air and materials

Alginate, sodium alginate in particular, is a natural polysaccharide derived from seaweed and has been widely used as a constituent of bioink in bioprinting[4-9,11,13] for its wide suitability as a versatile biomaterial.[35-38] Specifically, alginate can be chemically or physically modified to have various material properties including mechanical stiffness, swelling, degradation, cell attachment, and binding or release of bioactive molecules. For most bioprinting applications, a cell-laden alginate solution is directly printed into a calcium chloride or multivalent cation solution, which functions as the crosslinking as well as supporting solution as typical for support bath-based platform-assisted printing.[4,6,8,11] It has been a challenge to directly print 3D structures from a pre-mixed alginate and calcium chloride ink whose rheological properties are incompatible with bioprinting. For some applications, support bath-based printing is not realistic such as for *in situ* wound treatment printing where it is not practical to construct a support bath for printing locations. Fortunately, the proposed intersecting jets printing approach can be utilized for direct 3D printing in air using separate alginate and calcium chloride solutions.

Both acellular and cell-laden alginate structures were printed in air. For acellular structure printing, sodium alginate (Acros Organics, New Jersey, USA) was dissolved in DI water to 0.5% (w/v) as one ink, and calcium chloride dihydrate ($CaCl_2\bullet2H_2O$) (Sigma, St. Louis, MO) was dissolved in DI water to 5% (w/v) as the other ink. For cellular structure printing, 0.5%

sodium alginate was prepared in DMEM suspending NIH 3T3 mouse fibroblasts (ATCC, Rockville, MD) at a final concentration of 5×10^6 cells/mL. The 3T3 suspension was prepared in complete medium by following a protocol elsewhere.[6] This resulted in a 0.5% sodium alginate and 5×10^6 cells/mL cellular ink while the other ink is the 5% (w/v) calcium chloride dihydrate solution as for acellular structure printing. The droplet generation frequency for alginate solutions (acellular and cell-laden alginate solution) was 60 Hz, while the calcium chloride solution was deposited at 5 Hz to minimize the volume of excess fluid while ensuring complete crosslinking of the printed alginate. The structures were printed using a 1.0 mm/s printhead travel speed and a 25 μm layer thickness.

2.3.3. Compositional gradient printing and materials

Compositional gradients are ubiquitous in living organisms, providing heterogeneous microstructures/microenvironments to living cells of which they are composed. To illustrate the capability to print a structure which varies spatially in material composition, the proposed intersecting jets printing approach was implemented to fabricate a rectangular collagen sheet containing HAP nanoparticles, the concentration of which varied along the sheet thickness. Such sheets can be used as an interfacial structure between connective tissues, such as cartilage or tendon, and bone to promote functional regeneration of such interfaces.

Before fabrication, the HAP particles (nanopowder, Sigma-Aldrich, St. Louis, MO) were treated with a 1.62% (w/v) sodium citrate solution (Sigma-Aldrich, St. Louis, MO) to prevent settling and improve printability. Particles were then suspended in DI water and excess solids allowed to settle; the stable supernatant containing approximately 15 mg/mL citrate-treated HAP was then used as one of the two printing inks. An acidic collagen solution (rat tail type I, BD

Biosciences, Bedford, MA) at a concentration of 6 mg/mL was the other ink. Both of the inks were inkjet printed onto a platform at the surface of a PBS bath, which gelled the deposited collagen solution and encapsulated printed HAP particles. Some 5.00 × 5.00 × 0.75 mm square sheets were designed such that a three-tiered gradient in HAP content was formed across the thickness (0.75 mm) by adjusting the deposition rate of the HAP suspension. The droplet generation frequency for collagen solution was 60 Hz, while the HAP suspension was printed at 2, 10, and 20 Hz to result in different HAP concentrations in the three different layers. Structures were printed using a 3.3 mm/s printhead travel speed and a 50 μm layer thickness. After incubation for 24 hours to ensure complete gelation of the collagen component, constructs were frozen in liquid nitrogen, fractured to expose a cross-section through the thickness, freeze dried (FreeZone, Labconco, Kansas City, MO), and double-coated with carbon after mounting on a scanning electron microscope (SEM) specimen stub such that the cross section was available for imaging. The prepared samples were imaged and analyzed by energy dispersive spectroscopy using a desktop SEM (Phenom Pro-X, Phenom-World B.V., Eindhoven, Netherlands).

2.4. Assessment of cell viability and metabolic activity

NIH 3T3 cell viability in printed alginate constructs was assessed qualitatively using fluorescent staining and quantitatively using trypan blue exclusion. The control was the unprinted cellular ink as prepared. For fluorescence imaging, intact printed constructs were immersed in 100 μL PBS containing a final concentration of 10 μg/mL Hoechst 33342 (Molecular Probes, Eugene, OR) to stain nuclei blue, a final concentration of 10 μg/mL fluorescein diacetate (FDA) (Sigma-Aldrich, St. Louis, MO) to stain live cells green, and a final concentration of 2 μg/mL propidium iodide (PI) (Tocris Bioscience, Bristol, UK) to stain dead

cells red. After incubation in the dark for 5 minutes, images were captured using an EVOS FL inverted fluorescent microscope (ThermoFisher Scientific, Waltham, MA). For trypan blue assays, cell-laden constructs were liquefied using sterile 1.62% sodium citrate, and an aliquot of the resulting cell suspension was mixed with trypan blue (0.4%, Sigma-Aldrich, St. Louis, MO), which stains dead cells blue. 10 μL of this mixture was loaded on a standard hemocytometer, and the cell viability was determined by counting live (clear) and dead (blue) cells with an EVOS XL microscope (ThermoFisher Scientific, Waltham, MA).

Representative printed Puramatrix structures with encapsulated NSCs were transferred to complete medium supplemented with penicillin and streptomycin (Sigma-Aldrich, St. Louis, MO) for incubation. Fluorescent imaging was used to qualitatively assess cell viability and morphology by immersing structures in 100 μL PBS containing a final concentration of 10 μg/mL FDA to stain live cells green. After incubation in the dark for 5 minutes, images were captured using the EVOS FL inverted fluorescent microscope. The alamarBlue assay (ThermoFisher Scientific, Waltham, MA) was used to assess metabolic activity according the manufacturer's protocol, except the incubation period was extended to 18 hr; fluorescent intensity data was collected 1, 2, and 3 days after printing using a microplate reader (Synergy HT, Biotek, Winooski, VT).

3. Results and Discussion

3.1 Reactive material printing

3.1.1. NSC sphere printing

As shown in Fig. 3(a), NSCs suspended in PBS were deposited by one printhead while the other simultaneously deposited the acidic PuraMatrix hydrogel precursor solution. Droplets

mix and coalesce as the PuraMatrix precursor is rapidly crosslinked due to neutralization, encapsulating the NSCs within the PuraMatrix hydrogel with minimal exposure to the acidic environment. The PBS in the printed cell suspension aids in the gelation of the printed PuraMatrix hydrogel in addition to providing a cytocompatible and printable environment for the NSCs during printing. The PBS bath acts to support delicate printed structures during printing and facilitates gelation of the PuraMatrix precursor by supplying additional ions and buffering capacity to maintain a neutral pH. Fig. 3(c) shows a 3 mm diameter NSC sphere as printed. Fig. 3(d) shows a 2 mm diameter NSC sphere after 48 hours of incubation and FDA staining where green fluorescence indicates living cells. Printing time was approximately 3 minutes for 2 mm spheres and 9 minutes for 3 mm spheres.

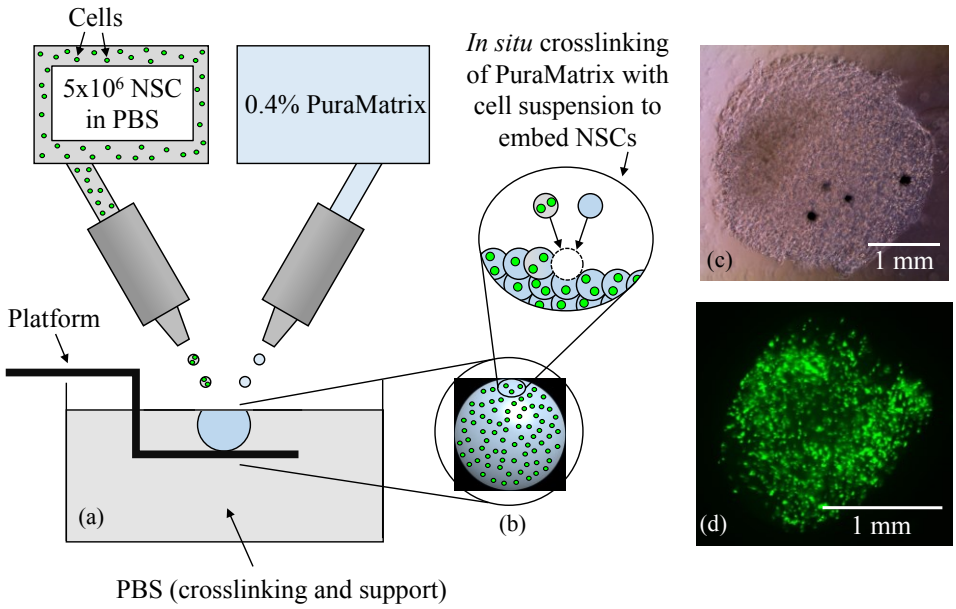

Fig. 3. (a) Intersecting jets approach for fabricating a PuraMatrix-based NSC sphere, (b) schematic of designed geometry, (c) 3 mm diameter sphere as printed, and (d) green fluorescent stain showing living cells within a 2 mm diameter NSC sphere.

In addition, disks of approximately 2 mm diameter and 1 mm thickness were fabricated under identical printing conditions to act as representative structures for cell morphology and metabolic activity assessment. Compared to spheres, disks offer improved nutrient diffusion throughout and a more planar distribution of cells for imaging. Both printed spheres and disks are found to retain their shape and are robust enough for handling over 7 days of culture. Since printed PuraMatrix structures are difficult to disrupt or dissolve, cell-counting-based viability tests were not attempted. Instead, NSCs are observed by fluorescent imaging to monitor the cell morphology during an incubation period of 7 days. Fig. 4(a) shows that cells are found to spread within the sphere during this period, indicating that the PuraMatrix structure provides a suitable environment for NSCs. While direct viability assays were not part of this study, the progressive changes in the cell morphology indicate that cells are alive and actively responding to their surroundings. Cell elongation and extension as shown in the inset are essential for cell-cell contacts and junctions which enable communication and guide tissue maturation. Over the incubation period a shift toward elongated morphologies instead of the initial round morphology are observed including stellate cells and long extensions between clusters. Analogous behavior has been observed for other neural cells maintained[39-41] and differentiated[42,43] in PuraMatrix. Additionally, metabolic activity increases as shown in Fig. 4(b) and a consistent increase is observed for each printed construct, indicating the suitability of the printed PuraMatrix structures for NSC culture.

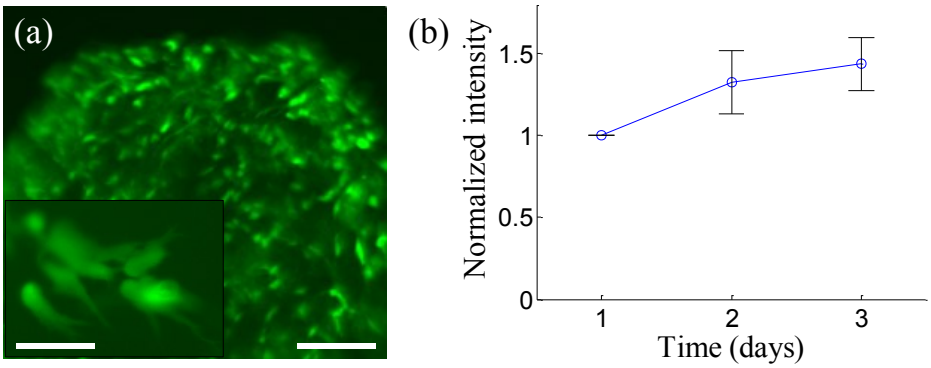

Fig. 4. (a) Fluorescent observation of printed cells with inset showing spreading after 7 days of culture (scale bars: 250 μm for main image and 25 μm for inset) and (b) normalized fluorescent alamarBlue intensity over three days of culture (error bars represent one standard deviation, n = 4).

3.1.2. Alginate structure printing in air

The simultaneous deposition of an acellular or fibroblast-laden alginate solution and a calcium chloride solution using intersecting jets enables the fabrication 3D structures directly in air to facilitate in situ printing applications. As shown in Fig. 5, printed droplets mix and coalesce on a substrate and alginate is crosslinked due to the presence of calcium cations. Due to the deposition of the crosslinking solution, hydrogel structures can be printed directly onto a glass slide rather than within a crosslinking bath as in previous studies.[4,6,8,11] Control of the distance between the printheads and substrate during printing is required, as jet intersection occurs at a specified location; for this reason, the receiving glass slide was lowered by the layer thickness as each layer was deposited. When solutions are deposited with different frequencies (60 Hz for alginate solution and 5 Hz for calcium chloride solution), the majority of alginate droplets being deposited do not intersect with a specific calcium droplet. However, crosslinking still occurs due to the diffusion of calcium throughout the structures. This is a particularly

interesting feature of this process; because droplets interact as they land on a receiving substrate, the droplet frequencies can be adjusted independently without necessarily influencing the shape fidelity of printed constructs. In contrast, for approaches involving mid-air droplet collisions, every pair of droplets must be precisely coordinated to achieve the desired final trajectory and the two jets must operate at the same frequency. Herein small amounts of excess fluid were wicked away from structures after printing. As expected, the absence of a supporting bath limits the achievable vertical height and complexity of printed gel structures due to their low mechanical stiffness.

Fig. 5(b) shows a 5 mm diameter acellular alginate tubular structure with a wall thickness around 1 mm, which was printed in 8 minutes. Fig. 5(c) illustrates connected 5 mm diameter annular structures with living cells, which were printed in 8 minutes. The dimensions of these constructs are suitable for organ-on-a-chip applications where small engineered constructs with controlled heterogeneity are necessary; direct printing of such constructs in air within chambers for more extensive cell studies may be the subject of future work. Because such chips often include sensitive electronic and mechanical components, immersing them in a crosslinking bath is undesirable.

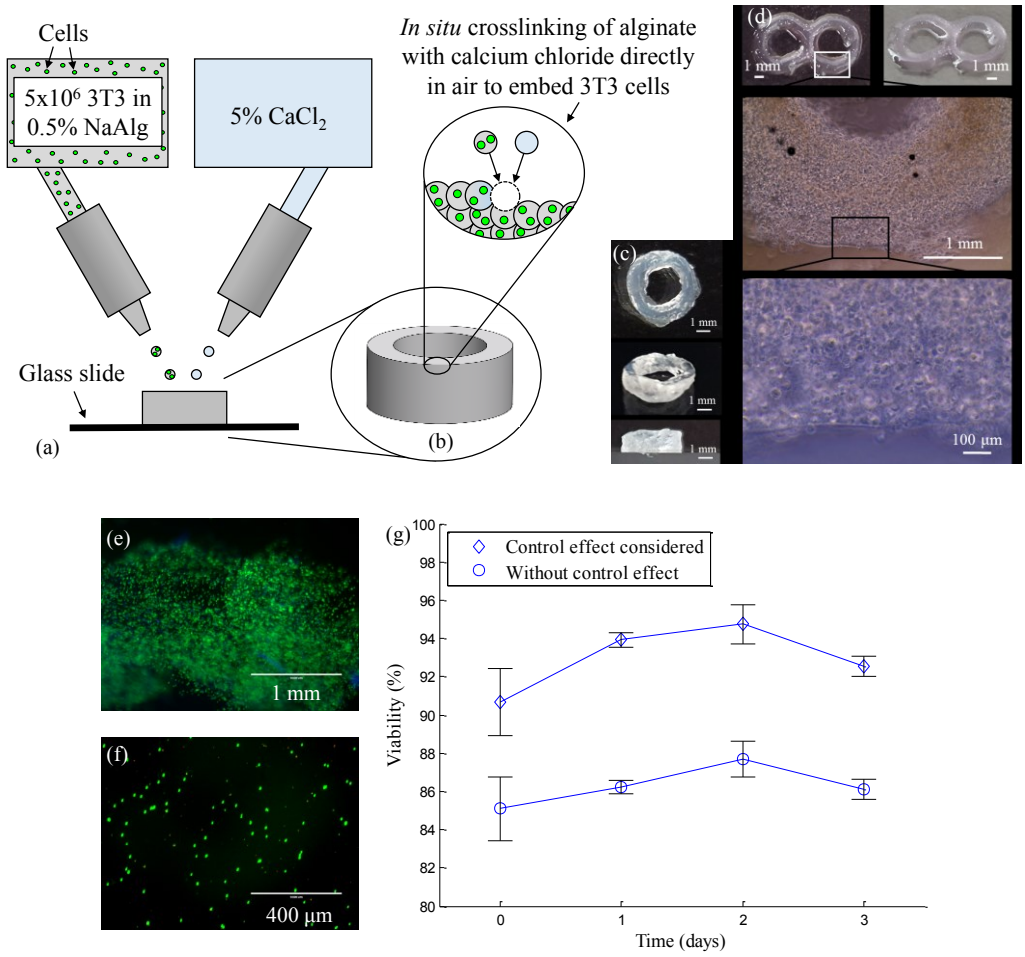

Fig. 5. (a) Intersecting jets for 3D inkjet printing in air, (b) schematic of designed structure, (c) a printed alginate-only tube, (d) printed cellular alginate annular structures, (e) fluorescence image of a printed tube with FDA and Hoechst 33342 stains, (f) fluorescence image of cells with FDA and PI stains after liquefaction for better imaging, and (g) cell viability measured immediately after printing and over 3 days of incubation (+/- one standard deviation).

Phase contrast microscopy in the Fig. 5(c) insets clearly shows the presence of cells within the walls of the structure. Fluorescence images in Fig. 5(d) and (e) show all cells in blue, many living cells in green, and few dead cells in red, indicating that the fabrication process is

mild and the vast majority of cells survive. To quantitatively evaluate the printing-induced cell death, the cell viability was evaluated using trypan blue. Cell viabilities immediately after printing and after 1, 2, and 3 days of incubation were 85.1%, 86.2%, 87.7%, and 86.1% without considering the control and 90.7%, 93.9%, 94.7%, and 92.5% considering the control effect, respectively. Such cell viability values are comparable to those reported elsewhere for inkjet bioprinting[6,8,44], indicating that printing in air is not significantly more damaging than bath-based printing. The initial increase is attributed to the post-printing proliferation, and the late decrease is attributed to cell death in the interior of the relatively thick walls of printed tubes due to limited oxygen and nutrition diffusion.

3.2. HAP compositional gradient printing

The intersecting jets approach was further used to fabricate collagen sheets with a gradient in HAP content along the thickness direction as shown in Fig. 6. Collagen and HAP jets intersect at the deposition location within a PBS bath, crosslinking the collagen and encapsulating printed HAP nanoparticles. The deposition frequency of the HAP jet during the fabrication of the lower third of the sheet was high, intermediate during the central third, and low during the upper third. This results in layers with HAP comprising 8%, 29%, and 45% of the total solids (HAP + collagen) by weight, effectively spanning the range of mineral density between soft tissues (~0%) and bone (~60%).[45] Some excess material buildup is observed at the periphery of printed sheets but structures largely captured their designed geometry and edge quality is not of primary concern for this study.

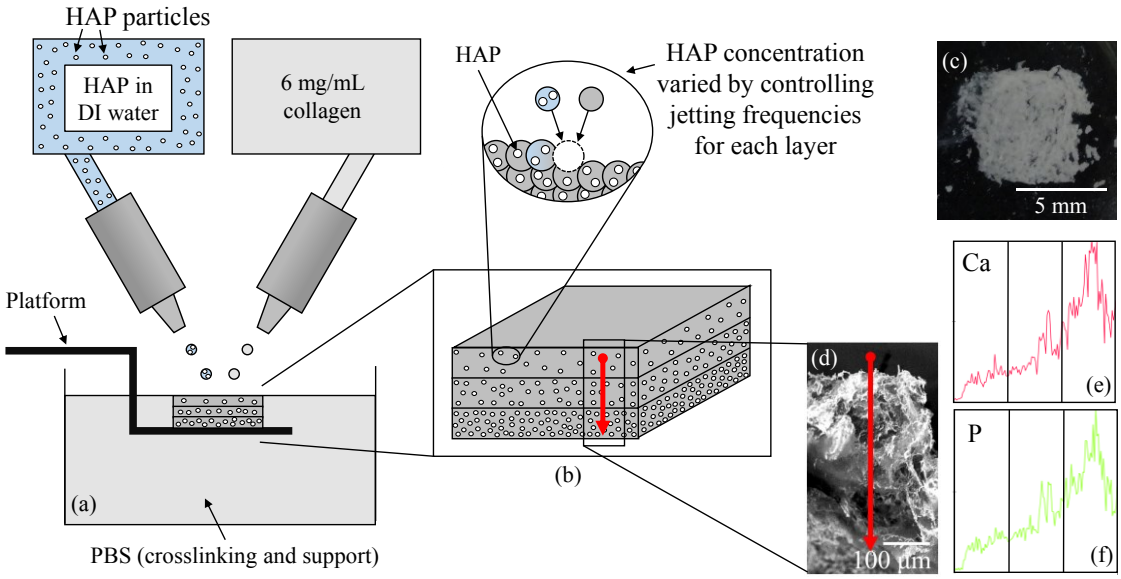

Fig. 6. (a) Intersecting jets approach for fabricating collagen sheet with a gradient in HAP content along the thickness direction, (b) schematic of designed structure, (c) top view of printed sheet, (d) EDS line scan location and SEM image, and (e, f) EDS results for calcium and phosphorous content indicating a gradient of HAP.

The structure was incubated under physiological conditions for 24 hours to ensure gelation of the collagen after printing. It was then prepared for SEM observation such that the field of view is a cross section of the sheet in order to observe the HAP gradient. Energy dispersive spectroscopy (EDS) was carried out using the SEM to measure the elemental composition along a specified path drawn across the sample thickness. Based on the chemical structure of HAP, its presence is indicated calcium (Ca) and phosphorous (P), which as shown in Fig. 6 (e, f) varies across the thickness of the collagen structure. Due to possible HAP sedimentation or droplet penetration during printing, the observed Ca and P concentrations increase linearly instead of stepwise.

4. Conclusions and future work

An intersecting jets-based inkjet printing approach has been developed and implemented to enable voxel-resolution printing-then-mixing for the fabrication of biological structures using reactive materials as well as structures having a compositional gradient. Two printheads are oriented such that they deposit droplets in the same location simultaneously, where printed solutions/suspensions actively mix and coalesce. The intersecting jets-based approach enables the fabrication of structures using reactive materials which cannot be mixed prior to deposition. That is, materials which undergo a loss of printability or cytocompatibility when mixed prior to deposition, as required by traditional printing approaches, are compatible with the proposed approach. Additionally, the intersecting jets approach offers online control of the local composition of printed structures. That is, structures with compositional gradients or arbitrarily varying material composition may be fabricated by controlling the ratio of deposited materials at any point within a structure.

To demonstrate reactive material printing, spheres encapsulating NSCs have been fabricated from a reactive PuraMatrix solution and a physiological cell suspension. Cells have remained viable through the printing process, spread within the matrix, and exhibited increased metabolic activity over 3 days of culture. Reactive material printing has also been utilized to print 3D cellular structures directly in air, rather than within a typically-used crosslinking bath, from alginate and calcium chloride solutions. The post-printing cell viability has remained above 90% over 3 days of culture, which is comparable to results reported elsewhere for inkjet bioprinting. To demonstrate the online control of material composition throughout structures, collagen sheets with a gradient in HAP content across their thickness have been fabricated from a collagen solution and HAP suspension. While the geometry of each designed structure has

been largely replicated, some imperfections have been observed. Lack of geometric fidelity is attributed to jetting inconsistencies innate to droplet-based printing of particle/cell-laden suspensions[46,47], and resulting geometries may be improved by reducing jetting variability. Structures generally have retained their printed shape during incubation, and significant swelling or shrinkage has not been observed.

Future work should aim to further improve the capabilities of the intersecting jets-based printing-then-mixing approach for the fabrication of structures using additional materials and with more complex geometries. In particular, automatic feedback control of nozzle alignment should be explored for robust printing implementation. High speed imaging should be used to quantify mixing dynamics and provide insight into droplet impact, mixing, and coalescence processes as well as the effects of printing conditions on the printing quality. Modeling and simulation approaches may also be implemented to elucidate the fundamental impact, spread, and mixing behavior of simultaneously deposited fluids. Regarding the application of 3D culture of NSCs in the matrix, further biological evaluation of their differentiation potentials into mature neurons or astrocytes will pave the way for future organoid generation. The geometric fidelity and complexity of structures printed directly in air should be improved. Finally, the osteoconductivity of printed HAP and collagen scaffolds and the effects of HAP gradient design should be investigated.

Acknowledgements

The authors have no conflict of interest to declare. This study was partially supported by the US National Science Foundation (CMMI-1634755). The authors would like to thank Dr. David

Wallace of MicroFab for the support of inkjetting setup implementation and Mr. Brian Davis of the University of Florida for his SEM support.

References

[1] Huang, Y.; Leu, M. C.; Mazumder, J.; Donmez, A. Additive manufacturing current state, future potential, gaps and needs, and recommendations. *Journal of Manufacturing Science and Engineering* **2015**, *137* (1), 014001, DOI: 10.1115/1.4028725.

[2] Murphy, S. V.; Atala, A. 3D bioprinting of tissues and organs. *Nat. Biotechnol.* **2014**, *32* (8), 773-785, DOI: 10.1038/nbt.2958.

[3] Ringeisen, B. R.; Pirlo, R. K.; Wu, P. K.; Boland, T.; Huang, Y.; Sun, W.; Hamid, Q.; Chrisey, D. B. Cell and organ printing turns 15 diverse research to commercial transitions *MRS Bull.* **2013**, *38* (10), 834-843, DOI: 10.1557/mrs.2013.209.

[4] Boland, T.; Tao, X.; Damon, B.J.; Manley, B.; Kesari. P.; Jalota, S.; Bhaduri, S. Drop on demand printing of cells and materials for designer tissue constructs *Mater. Sci. Eng., C* **2007**, *27*, 372-376, DOI: 10.1016/j.msec.2006.05.047.

[5] Nishiyama, Y.; Nakamura, M.; Henmi, C.; Yamaguchi, K.; Mochizuki, S. Nakagawa, H.; Takiura, K. Development of a three-dimensional bioprinter construction of cell supporting structures using hydrogel and state-of-the-art inkjet technology *J. Biomech. Eng.* **2009**, *131*, 035001, DOI: 10.1115/1.3002759.

[6] Xu, C.; Chai, W.; Huang, Y.; Markwald, R. R. Scaffold-free inkjet printing of three-dimensional zigzag cellular tubes *Biotechnol. Bioeng.* **2012**, *109* (12), 3152-3160, DOI: 10.1002/bit.24591.

[7] Xu, T.; Zhao, W.; Zhu, J. M.; Albanna, M. Z.; Yoo, J. J., Atala, A. Complex heterogeneous tissue constructs containing multiple cell types prepared by inkjet printing technology *Biomaterials* **2013** *34* (1), 130-139, DOI: 10.1016/j.biomaterials.2012.09.035.

[8] Christensen, K.; Xu, C.; Chai, W.; Zhang, Z.; Fu, J.; Huang, Y. Freeform inkjet printing of cellular structures with bifurcations *Biotechnol. Bioeng.* **2015**, *112*, 1047-1055, DOI: 10.1002/bit.25501.

[9] Compaan, A. M.; Christensen, K.; Huang, Y. Inkjet bioprinting of 3D silk fibroin cellular constructs using sacrificial alginate *ACS Biomater. Sci. Eng.* **2016**, *3* (8), 1519-1526, DOI: 10.1021/acsbiomaterials.6b00432.

[10] Yan, J.; Huang, Y.; Chrisey, D. B. Laser-assisted printing of alginate long tubes and annular constructs *Biofabrication* **2013**, *5* (1), 015002, DOI: 10.1088/1758-5082/5/1/015002.

[11] Xiong, R.; Zhang, Z.; Chai, W.; Huang, Y.; Chrisey, D. B. Freeform drop-on-demand laser printing of 3D alginate and cellular constructs *Biofabrication* **2015**, *7* (4), 045011, DOI: 10.1088/1758-5090/7/4/045011.

[12] Duan, B.; Hockaday, L. A.; Kang, K. H.; Butcher, J. T. 3D bioprinting of heterogeneous aortic valve conduits with alginate/gelatin hydrogels *J. Biomed. Mater. Res., Part A* **2013**, *101* (5), 1255-1264, DOI: 10.1002/jbm.a.34420.

[13] Jin, Y.; Compaan, A.; Bhattacharjee, T.; Huang, Y. Granular gel support-enabled extrusion of three-dimensional alginate and cellular structures *Biofabrication* **2016**, *8* (2), 025016, DOI: 10.1088/1758-5090/8/2/025016.

[14] Norotte, C.; Marga, F. S.; Niklason, L. E.; Forgacs, G. Scaffold-free vascular tissue engineering using bioprinting *Biomaterials* **2009**, *30* (30), 5910-5917, DOI: 10.1016/j.biomaterials.2009.06.034.

[15] Skardal, A.; Zhang, J.; Prestwich, G. D. Bioprinting vessel-like constructs using hyaluronan hydrogels crosslinked with tetrahedral polyethylene glycol tetracrylates *Biomaterials* **2010**, *31* (24), 6173-6181, DOI: 10.1016/j.biomaterials.2010.04.045.

[16] Faulkner-Jones, A.; Greenhough, S.; King, J. A.; Gardner, J.; Courtney, A.; Shu, W. Development of a valve-based cell printer for the formation of human embryonic stem cell spheroid aggregates *Biofabrication* **2013**, *5* (1), 015013, DOI: 10.1088/1758-5082/5/1/015013.

[17] Faulkner-Jones, A.; Fyfe, C.; Cornelissen, D. J.; Gardner, J.; King, J.; Courtney, A.; Shu, W. Bioprinting of human pluripotent stem cells and their directed differentiation into hepatocyte-like cells for the generation of mini-livers in 3D *Biofabrication* **2015**, *7* (4), 044102, DOI: 10.1088/1758-5090/7/4/044102.

[18] Li, C.; Faulkner-Jones, A.; Dun, A. R.; Jin, J.; Chen, P.; Xing, Y.; Yang, Z.; Li, Z.; Shu, W.; Liu, D.; Duncan, R. R. Rapid formation of a supramolecular polypeptide–DNA hydrogel for in situ three-dimensional multilayer bioprinting *Angew. Chem., Int. Ed.* **2015**, *54* (13), 3957-3961, DOI: 10.1002/anie.201411383.

[19] Fathi, S.; Dickens, P. Challenges in drop-on-drop deposition of reactive molten nylon materials for additive manufacturing *J. Mater. Process. Technol.* **2013**, *213* (1), 84-93, DOI: 10.1016/j.jmatprotec.2012.08.006.

[20] Yeo, Y.; Chen, A. U.; Basaran, O. A.; Park, K. Solvent exchange method a novel microencapsulation technique using dual microdispensers *Pharm. Res.* **2004**, *21* (8), 1419-1427, DOI: 10.1023/B:PHAM.0000036916.96307.d8.

[21] Yeo, Y.; Park, K. A new microencapsulation method using an ultrasonic atomizer based on interfacial solvent exchange *J. Controlled Release* **2004**, *100* (3), 379-388, DOI: 10.1016/j.jconrel.2004.09.012.

[22] Park, J. H.; Ye, M.; Yeo, Y.; Lee, W. K.; Paul, C.; Park, K. Reservoir-type microcapsules prepared by the solvent exchange method effect of formulation parameters on microencapsulation of lysozyme *Mol. Pharmaceutics* **2006**, *3* (2), 135-143, DOI: 10.1021/mp050083w.

[23] Mou, F.; Chen, C.; Guan, J.; Chen, D. R.; Jing, H. Oppositely charged twin-head electrospray a general strategy for building Janus particles with controlled structures *Nanoscale* **2013**, *5* (5), 2055-2064, DOI: 10.1039/C2NR33523A.

[24] Wan, F.; Maltesen, M. J.; Andersen, S. K.; Bjerregaard, S.; Foged, C.; Rantanen, J.; Yang, M. One-step production of protein-loaded PLGA microparticles via spray drying using 3-fluid nozzle *Pharm. Res.* **2014**, *31* (8), 1967-1977, DOI: 10.1007/s11095-014-1299-1.

[25] Xu, F.; Celli, J.; Rizvi, I.; Moon, S.; Hasan, T.; Demirci, U. A three-dimensional in vitro ovarian cancer coculture model using a high-throughput cell patterning platform *Biotechnol. J.* **2011**, *6* (2), 204-212, DOI: 10.1002/biot.201000340.

[26] Campbell, P. G.; Miller, E. D.; Fisher, G. W.; Walker, L. M.; Weiss, L. E. Engineered spatial patterns of FGF-2 immobilized on fibrin direct cell organization *Biomaterials* **2005**, *26* (33), 6762-6770, DOI: 10.1016/j.biomaterials.2005.04.032.

[27] Phillippi, J. A.; Miller, E.; Weiss, L.; Huard, J.; Waggoner, A.; Campbell, P. Microenvironments engineered by inkjet bioprinting spatially direct adult stem cells toward muscle-and bone-like subpopulations *Stem Cells* **2008**, *26* (1), 127-134, DOI: 10.1634/stemcells.2007-0520.

[28] Ober, T. J.; Foresti, D.; Lewis, J. A. Active mixing of complex fluids at the microscale *Proc. Natl. Acad. Sci. U. S. A.* **2015**, *112* (40), 12293-12298, DOI: 10.1073/pnas.1509224112.

[29] Herran, C. L.; Huang, Y.; Chai, W. Performance evaluation of bipolar and tripolar excitations during nozzle-jetting-based alginate microsphere fabrication *J. Micromech. Microeng.* **2012**, *22* (8), 085025-1-11, DOI: 10.1088/0960-1317/22/8/085025.

[30] Thornhoff, J. R.; Lou, D. I.; Jordan, P. M.; Zhao, X.; Wu, P. Compatibility of human fetal neural stem cells with hydrogel biomaterials in vitro *Brain Res.* **2007**, *1187*, 42-51, DOI: 10.1016/j.brainres.2007.10.046.

[31] Allen, P.; Melero-Martin, J.; Bischoff, J. Type I collagen, fibrin and PuraMatrix matrices provide permissive environments for human endothelial and mesenchymal progenitor cells to form neovascular networks *J. Tissue Eng. Regener. Med.* **2011**, *5*, 74-86, DOI: 10.1002/term.389.

[32] Li, X.; Katsanevakis, E.; Liu, X.; Zhang, N.; Wen, X. Engineering neural stem cell fates with hydrogel design for central nervous system regeneration *Prog. Polym. Sci.* **2012**, *37*, 1105-1129, DOI: 10.1016/j.progpolymsci.2012.02.004.

[33] Xia, G.; Santostefano, K. E.; Goodwin, M.; Liu, J.; Subramony, S. H.; Swanson, M. S.; Terada, N.; Ashizawa, T. Generation of neural cells from DM1 induced pluripotent stem cells as cellular model for the study of central nervous system neuropathogenesis *Cell. Reprogram.* **2013**, *15*, 166-177, DOI: 10.1089/cell.2012.0086.

[34] Xia, G.; Ashizawa, T. Dynamic changes of nuclear RNA foci in proliferating DM1 cells *Histochem. Cell Biol.* **2015**, *143*, 557-564, DOI: 10.1007/s00418-015-1315-5.

[35] Augst, A. D.; Kong, H. J.; Mooney, D. J. Alginate hydrogels as biomaterials *Macromol. Biosci.* **2006**, *6*, 623-633, DOI: 10.1002/mabi.200600069.

[36] Murphy, S. V.; Skardal, A.; Atala, A. Evaluation of hydrogels for bio-printing applications *J. Biomed. Mater. Res., Part A* **2013**, *101*, 272-284, DOI: 10.1002/jbm.a.34326.

[37] Fan, L.; Cao, M.; Gao, S.; Wang, T.; Wu, H.; Peng, M.; Zhou, X.; Nie, M. Preparation and characterization of sodium alginate modified with collagen peptides *Carbohydr. Polym.* **2013**, *93* (2), 380-385, DOI: 10.1016/j.carbpol.2013.01.029.

[38] Sun, J.; Tan, H. Alginate-based biomaterials for regenerative medicine applications *Materials* **2013**, *6* (4), 1285-1309, DOI: 10.3390/ma6041285.

[39] Aligholi, H.; Rezayat, S. M.; Azari, H.; Mehr, S. E.; Akbari, M.; Mousavi, S. M. M.; Attari, F.; Alipour, F.; Hassanzadeh, G.; Gorji, A. Preparing neural stem/progenitor cells in PuraMatrix hydrogel for transplantation after brain injury in rats a comparative methodological study *Brain Res.* **2016**, *1642*, 197-208, DOI: 10.1016/j.brainres.2016.03.043.

[40] Curley, J. L.; Sklare, S. C.; Bowser, D. A.; Saksena, J.; Moore, M. J.; Chrisey, D. B. Isolated node engineering of neuronal systems using laser direct write *Biofabrication* **2016**, *8* (1), 015013, DOI: 10.1088/1758-5090/8/1/015013.

[41] Negah, S. S.; Khaksar, Z.; Aligholi, H.; Sadeghi, S. M.; Mousavi, S. M. M.; Kazemi, H.; Jahan-Abad, A. J.; Gorji, A. Enhancement of neural stem cell survival, proliferation, migration, and differentiation in a novel self-assembly peptide nanofibber scaffold *Mol. Neurobiol.* **2016**, 1-13, DOI: 10.1007/s12035-016-0295-3.

[42] Ni, N.; Hu, Y.; Ren, H.; Luo, C.; Li, P.; Wan, J. B.; Su, H. Self-assembling peptide nanofiber scaffolds enhance dopaminergic differentiation of mouse pluripotent stem cells in 3-dimensional culture *PloS One* **2013**, *8* (12), e84504, DOI: 10.1371/journal.pone.0084504.

[43] Francis, N. L.; Bennett, N. K.; Halikere, A.; Pang, Z. P.; Moghe, P. V. Self-assembling peptide nanofiber scaffolds for 3-D reprogramming and transplantation of human pluripotent stem cell-derived neurons *ACS Biomater. Sci. Eng.* **2016**, *2* (6), 1030-1038, DOI: 10.1021/acsbiomaterials.6b00156.

[44] Xu, T.; Jin, J.; Gregory, C.; Hickman, J. J.; Boland, T. Inkjet printing of viable mammalian cells *Biomaterials* **2005**, *26* (1), 93-99, DOI: 10.1016/j.biomaterials.2004.04.011.

[45] Boskey, A. L. Bone composition: relationship to bone fragility and antiosteoporotic drug effects *BoneKEy Rep.* **2013**, *2*, 447, DOI: 10.1038/bonekey.2013.181.

[46] Xu, C.; Zhang, M.; Huang, Y.; Ogale, A.; Fu, J.; Markwald, R. R. Study of droplet formation process during drop-on-demand inkjetting of living cell-laden bioink *Langmuir* **2014**, *30*, 9130-9138, DOI: 10.1021/la501430x.

[47] Zhang, Z.; Xu, C.; Xiong, R.; Chrisey, D. B.; Huang, Y. Effects of living cells on the bioink printability during laser printing *Biomicrofluidics* **2017**, *11* (3), 034120-1-16, DOI: 10.1063/1.4985652.